Research Article | Vol. 29, No. 12 / 7 June 2021 / Optics Express 18611
Optics EXPRESS

Efficient HIE-FDTD method for designing a dual-band anisotropic terahertz absorption structure

YUANGUO ZHOU,[1] HANG LI,[1] LI LI,[2,5] YIJUN CAI,[3,6] KIRILL ZEYDE,[4] AND XIAOBING HAN[1]

[1]College of Communication and Information Engineering, Xi'an University of Science and Technology, Xi'an 710054, China
[2]Kuang-Chi Institute of Advanced Technology, Shenzhen 518000, China
[3]Fujian Provincial Key Laboratory of Optoelectronic Technology and Devices, Xiamen University of Technology, Xiamen 361024, China
[4]Department of Radioelectronics and Telecommunication, Ural Federal University, Yekaterinburg 620002, Russia
[5]lifunnyxast@foxmail.com
[6]yijuncai@foxmail.com

Abstract: The finite-difference time-domain (FDTD) method is considered to be one of the most accurate and common methods for the simulation of optical devices. However, the conventional FDTD method is subject to the Courant-Friedrich-Levy condition, resulting in extremely low efficiency for calculating two-dimensional materials (2DMs). Recent researches on the hybrid implicit-explicit FDTD (HIE-FDTD) method show that the method can efficiently simulate homogeneous and isotropic 2DMs such as graphene sheet; however, it is inapplicable to the anisotropic medium. In this paper, we propose an in-plane anisotropic HIE-FDTD method to simulate optical devices containing graphene and black phosphorus (BP) sheets. Numerical analysis shows that the proposed method is accurate and efficient. With this method, we present a novel multi-layer graphene-BP-based dual-band anisotropic terahertz absorption structure (GBP-DATAS) and analyze its optical characteristics. Combining the advantages of graphene and BP localized surface plasmons, the GBP-DATAS demonstrates strong anisotropic plasmonic resonance and high absorption rate in the terahertz band.

1. Introduction

The emerging two-dimensional materials (2DMs) exhibit a wide range of electronic properties and attract extensive attentions due to their huge potentials in application of electronic and photonic devices [1,2]. Among various 2DMs, graphene has drawn a surge of interest in both academia and industry due to its unique properties [3–10]. However, graphene is also limited in many aspects due to its inherent zero band gap structure [11]. Recently, the rise of black phosphorus (BP) research shows that it can faultlessly fill in the gap left by other 2DMs [12]. BP is an in-plane anisotropic nanomaterial of which unique photoelectric properties have promoted its application in many fields, for example, physical and chemical field [13–18]. As a result, BP transistors, antennas and surface plasmonic devices spring up in recent years [19–21]. Nevertheless, due to limitations in preparation and detection process, development and performance measurement of graphene and BP shall be realized relying on complex nano manufacturing and measuring instruments. To calculate optical properties of graphene, various simulation algorithms have been developed, such as the finite-different time-domain (FDTD) [22–26], hybrid implicit-explicit FDTD (HIE-FDTD) [27–32], alternating direction implicit FDTD (ADI-FDTD) [33,34], and locally one-dimensional FDTD (LOD-FDTD) [35,36]. However, few numerical methods can be used to simulate black phosphorus due to its in-plane anisotropic characteristics, designing

#427420 https://doi.org/10.1364/OE.427420
Journal © 2021 Received 12 Apr 2021; revised 7 May 2021; accepted 18 May 2021; published 1 Jun 2021

Optics EXPRESS

BP devices with efficient algorithm has become one of the urgent problems to be solved in nowadays. The existing approach to simulate black phosphorus is the conventional FDTD method [37,38], combined with monolayer BP Drude model with frequency up to 10 THz and the auxiliary differential equation (ADE) technique. Despite it has high precision in calculation, the conventional FDTD method is greatly limited in efficiency, resulting in more calculation time and memory consumption, because the BP and graphene sheets only have atomic-scale thickness which require a mass of numerical discretization due to the Courant-Friedrich-Levy (CFL) condition in the FDTD scheme [39].

Several implicit methods have been proposed to overcome limitations of the CFL condition in the FDTD method. The implicit differential methods, such as the ADI-FDTD and the Crank-Nicolson FDTD (CN-FDTD) methods [40,41], are unconditionally stable, of which time step are only limited by numerical error and have no correlation with the spatial step. However, they also have many dominant disadvantages, that is to say, the inversion of large-scale matrix must be solved, resulting in a lot of calculation work and low efficiency. On the other hand, although the hybrid implicit-explicit FDTD (HIE-FDTD) method is not unconditionally stable like the ADI-FDTD method, its CFL condition only depends on the size of spatial discretization in two directions, which can effectively avoid limitation of minimum spatial discretization to time step. Therefore, the HIE-FDTD method is well-suited for simulating materials with two-dimensional structures, for example, the graphene and BP sheets.

However, the existing HIE-FDTD methods are mainly applicable to homogeneous and isotropic medium, where HIE-FDTD is used for research on the application of hybrid electromagnetic system [42], application of microstrip circuit [43], application of graphene absorber [44], application of calculating shielding efficiency of thin-wall shell [45], and application of antenna with precise dimension [46], etc. In this paper, an efficient in-plane anisotropic HIE-FDTD method is proposed to simulate the photoelectric properties of the black phosphorus. With the proposed method, it is possible to simulate devices containing graphene and BP sheets. In addition, in order to simulate 2DMs with curved structure more accurately, a conformal technology for anisotropic HIE-FDTD method is proposed here to improve the computational accuracy and efficiency and reduce the consumption [47].

Based on the anisotropic HIE-FDTD technology, we propose a novel graphene-BP-based dual-band anisotropic terahertz absorption structure (GBP-DATAS). The GBP-DATAS employs plasmonic feature of the graphene-BP and demonstrates strong anisotropic plasma resonance which cannot be realized in a single graphene or BP layer. Through multi-layer graphene-BP stacking, the GBP-DATAS can generate a dual-band absorption peak and reach an absorption rate up to 100% in the terahertz band. In addition, it is possible to get different absorption spectrum through adjusting geometrical parameters and doping level of the structure. The physical mechanism is also analyzed through the electromagnetic field distribution calculated by the proposed HIE-FDTD method.

The remainder of the paper is organized as follows. Section 2 infers the dispersive and in-plane anisotropic HIE-FDTD formula by the Drude model combining with the ADE technique, and represents the conformal HIE-FDTD updating equations which is applicable to the simulation of curved structure. Section 3 simulates the multi-layer GBP-DATAS with the proposed method and provides related numerical results and analyses. Finally, Section 4 briefly concludes the paper.

Optics EXPRESS

2. Methodology

2.1. Dispersive characteristic of graphene

The electric conductivity of graphene can be described by the Drude model in microwave and terahertz frequency range [31,32]

$$\sigma_g(\omega) = \frac{\tau e^2 k_B T}{\pi\hbar^2(1+j\omega\tau)}\left(\frac{\mu_c}{k_B T} + 2\ln\left[1+\exp\left(-\frac{\mu_c}{k_B T}\right)\right]\right) \tag{1}$$

where ω is the angular frequency of the incident light, $\hbar$ is the reduced Planck constant, e is the electron charge, k_B is the Boltzmann constant, T is the temperature in Kelvin, μ_c is the chemical potential, $\tau = 1/(2\kappa)$ is the phenomenological scattering time, and κ is the scattering rate.

Assume that the graphene thickness is expressed as d, then the relative permittivity can be described as

$$\varepsilon_r(\omega) = 1 - j\sigma_g(\omega)/\omega\varepsilon_0 d \tag{2}$$

In order to model the dispersive feature of the graphene, the conduction current density of J is introduced to represent graphene's conductivity.

$$J(\omega) = \sigma_g(\omega)E(\omega)/d \tag{3}$$

Separate frequency term from conductivity σ_g, (3) can be rewritten as

$$J(\omega) + j\omega\tau J(\omega) = \sigma_0 E(\omega)/d \tag{4}$$

where

$$\sigma_0(\omega) = \frac{\tau e^2 k_B T}{\pi\hbar^2}\left(\frac{\mu_c}{k_B T} + 2\ln\left[1+\exp\left(-\frac{\mu_c}{k_B T}\right)\right]\right)$$

By transforming (4) into time domain and replacing the time derivative with centered second-order finite differences, we can obtain

$$J_x^{n+1} = S_1 J_x^n + S_2 E_x^{n+1} + S_2 E_x^n \tag{5}$$

$$J_y^{n+1} = S_1 J_y^n + S_3 E_y^{n+1} + S_3 E_y^n \tag{6}$$

where

$$S_1 = \frac{2\tau - \Delta t}{2\tau + \Delta t}, \quad S_2 = \frac{\sigma_0 \Delta t}{(2\tau + \Delta t)d}, \quad S_3 = \frac{\sigma_0 \Delta t}{(2\tau + \Delta t)d}$$

Equations (5) and (6) represent the dispersive characteristic of the graphene, which can be introduced into the HIE-FDTD method easily.

2.2. Anisotropic conductivity of black phosphorus

The monolayer BP shows in-plane anisotropic properties which is mainly caused by the surface conductivity. From the semiclassical Drude model, the value of surface conductivity in the mid-IR and far-IR wavelength regimes can be characterized as a diagonal tensor

$$\bar{\bar{\sigma}}_{BP} = \begin{pmatrix} \dfrac{je^2 n_s}{(\omega + j\eta/\hbar)m_{cx}} & 0 \\ 0 & \dfrac{je^2 n_s}{(\omega + j\eta/\hbar)m_{cy}} \end{pmatrix} \tag{7}$$

Optics EXPRESS

where η is the parameter describing the relaxation rate, n_s describes the electron doping. The electron mass along the x-direction and y-direction can be described by [13]

$$m_{cx} = \hbar^2/\left(2\gamma^2/\Delta + \eta_c\right), \quad m_{cy} = \hbar^2/v_c \tag{8}$$

Here, for monolayer BP, we have $\gamma = 4a/\pi$ eVm, $V_c = \hbar^2/(0.7m_0)$, $\eta_c = \hbar^2/(0.4m_0)$, and the band gap $\Delta = 2$ eV, for a standard electron rest mass $m_0 = 9.10938 \times 10^{-31}$kg. a denotes the scale length of the BP and π/a denotes the width of the Brillouin Zone.

Separate frequency term from conductivity $\bar{\bar{\sigma}}_{BP}$, (7) can be rewritten as

$$\bar{\bar{\sigma}}_{BP} = \frac{1}{\eta - j\omega\hbar}\begin{pmatrix} \sigma_{cx} & 0 \\ 0 & \sigma_{cy} \end{pmatrix} \tag{9}$$

where

$$\sigma_{cx} = \hbar e^2 n_s/m_{cx}, \quad \sigma_{cy} = \hbar e^2 n_s/m_{cy}$$

For a single layer BP sheet with thickness h, the relation between the conduction current density of $\tilde{J}$ and the electric field of E can be described as

$$\begin{pmatrix} \tilde{J}_x \\ \tilde{J}_y \end{pmatrix} = \frac{1}{h}\bar{\bar{\sigma}}_{BP}\begin{pmatrix} E_x \\ E_y \end{pmatrix} \tag{10}$$

Substituting (9) into (10), it obtains

$$-j\omega\hbar\tilde{J}_x(\omega) + \eta\tilde{J}_x(\omega) = \sigma_{cx}E_x(\omega)/h \tag{11}$$

$$-j\omega\hbar\tilde{J}_y(\omega) + \eta\tilde{J}_y(\omega) = \sigma_{cy}E_y(\omega)/h \tag{12}$$

By transforming (11) and (12) into time domain and replacing the time derivative with centered second-order finite differences, we have

$$-\frac{\hbar}{\Delta t}\left(\tilde{J}_x^{n+1} - \tilde{J}_x^n\right) + \frac{\eta}{2}\left(\tilde{J}_x^{n+1} + \tilde{J}_x^n\right) = \frac{\sigma_{cx}}{2h}\left(E_x^{n+1} + E_x^n\right) \tag{13}$$

$$-\frac{\hbar}{\Delta t}\left(\tilde{J}_y^{n+1} - \tilde{J}_y^n\right) + \frac{\eta}{2}\left(\tilde{J}_y^{n+1} + \tilde{J}_y^n\right) = \frac{\sigma_{cy}}{2h}\left(E_y^{n+1} + E_y^n\right) \tag{14}$$

Rearrangement of (13) and (14) leads to

$$\tilde{J}_x^{n+1} = C_1\tilde{J}_x^n + C_2E_x^{n+1} + C_2E_x^n \tag{15}$$

$$\tilde{J}_y^{n+1} = C_1\tilde{J}_y^n + C_3E_y^{n+1} + C_3E_y^n \tag{16}$$

where

$$C_1 = \frac{2\hbar + \Delta t\eta}{2\hbar - \Delta t\eta}, \quad C_2 = -\frac{\Delta t\sigma_{cx}}{(2\hbar - \Delta t\eta)h}, \quad C_3 = -\frac{\Delta t\sigma_{cy}}{(2\hbar - \Delta t\eta)h}$$

Equations (15) and (16) represent the dispersive and anisotropic characteristic of the black phosphorus, which can also be introduced into the HIE-FDTD method easily.

Optics EXPRESS

2.3. Formulas of the HIE-FDTD method

To model system involving both graphene and BP sheet, the conduction current densities of J and $\tilde{J}$ induced by graphene and BP, respectively, are introduced to the HIE-FDTD method. By incorporating the ADEs (5-6) and (15-16) into Maxwell's equations and applying the hybrid implicit explicit difference scheme, the iterative formulations for the dispersive and anisotropic HIE-FDTD method are as follows

$$E_x^{n+1} = E_x^n + \frac{\Delta t}{\varepsilon_0}\ell_y H_z^n - \frac{\Delta t}{2\varepsilon_0}\ell_z\left(H_y^n + H_y^{n+1}\right) - \frac{\Delta t}{2\varepsilon_0}\left(J_x^n + J_x^{n+1}\right) - \frac{\Delta t}{2\varepsilon_0}\left(\tilde{J}_x^n + \tilde{J}_x^{n+1}\right) \tag{17a}$$

$$E_y^{n+1} = E_y^n - \frac{\Delta t}{\varepsilon_0}\ell_x H_z^n + \frac{\Delta t}{2\varepsilon_0}\ell_z\left(H_x^n + H_x^{n+1}\right) - \frac{\Delta t}{2\varepsilon_0}\left(J_y^n + J_y^{n+1}\right) - \frac{\Delta t}{2\varepsilon_0}\left(\tilde{J}_y^n + \tilde{J}_y^{n+1}\right) \tag{17b}$$

$$E_z^{n+1} = E_z^n + \frac{\Delta t}{\varepsilon_0}\ell_x H_y^n - \frac{\Delta t}{\varepsilon_0}\ell_y H_x^n \tag{17c}$$

$$H_x^{n+1} = H_x^n - \frac{\Delta t}{\mu_0}\ell_y E_z^n + \frac{\Delta t}{2\mu_0}\ell_z\left(E_y^n + E_y^{n+1}\right) \tag{17d}$$

$$H_y^{n+1} = H_y^n + \frac{\Delta t}{\mu_0}\ell_x E_z^n - \frac{\Delta t}{2\mu_0}\ell_z\left(E_x^n + E_x^{n+1}\right) \tag{17e}$$

$$H_z^{n+1} = H_z^n - \frac{\Delta t}{\mu_0}\ell_x E_y^n + \frac{\Delta t}{\mu_0}\ell_y E_x^n \tag{17f}$$

From (17a) and (17b), we note that the updating of E_x^{n+1} and E_y^{n+1} needs the unknown H_y^{n+1}, J_x^{n+1}, $\tilde{J}_x^{n+1}$ and H_x^{n+1}, J_y^{n+1}, $\tilde{J}_y^{n+1}$ at the same time. Therefore, the components E_x^{n+1} and E_y^{n+1} would be calculated implicitly.

Using (5) and (15) to replace J_x^{n+1} and $\tilde{J}_x^{n+1}$, respectively, and substituting (17e) into (17a), the update formula for E_x^{n+1} can be derived

$$\begin{aligned}\left[1 - \frac{\Delta t^2}{4\varepsilon_0\mu_0}\ell_z^2 + \frac{\Delta t}{2\varepsilon_0}\left(S_2 + C_2\right)\right]E_x^{n+1} &= \left[1 + \frac{\Delta t^2}{4\varepsilon_0\mu_0}\ell_z^2 - \frac{\Delta t}{2\varepsilon_0}\left(S_2 + C_2\right)\right]E_x^n \\ -\frac{\Delta t^2}{2\varepsilon_0\mu_0}\ell_z\ell_x E_z^n - \frac{\Delta t}{\varepsilon_0}\left(\ell_z H_y^n - \ell_y H_z^n\right) &- \frac{\Delta t}{2\varepsilon_0}\left(1 + S_1\right)J_x^n - \frac{\Delta t}{2\varepsilon_0}\left(1 + C_1\right)\tilde{J}_x^n\end{aligned} \tag{18}$$

Using (6) and (16) to replace J_y^{n+1} and $\tilde{J}_y^{n+1}$, respectively, and substituting (17d) into (17b), the update formula for E_y^{n+1} can be derived

$$\begin{aligned}\left[1 - \frac{\Delta t^2}{4\varepsilon_0\mu_0}\ell_z^2 + \frac{\Delta t}{2\varepsilon_0}\left(S_3 + C_3\right)\right]E_y^{n+1} &= \left[1 + \frac{\Delta t^2}{4\varepsilon_0\mu_0}\ell_z^2 - \frac{\Delta t}{2\varepsilon_0}\left(S_3 + C_3\right)\right]E_y^n \\ -\frac{\Delta t^2}{2\varepsilon_0\mu_0}\ell_z\ell_y E_z^n - \frac{\Delta t}{\varepsilon_0}\left(\ell_x H_z^n - \ell_z H_x^n\right) &- \frac{\Delta t}{2\varepsilon_0}\left(1 + S_1\right)J_y^n - \frac{\Delta t}{2\varepsilon_0}\left(1 + C_1\right)\tilde{J}_y^n\end{aligned} \tag{19}$$

Equations (18), (19), (17c)–(17f) are the final anisotropic HIE-FDTD formulas that can be utilized to simulate system involving both graphene and BP sheet efficiently. From the above equations we can see that, in the graphene cells the current density $\tilde{J}$ induced by BP is equal to zero, C_2 and C_3 are also equal to zero due to the absence of σ_{cx} and σ_{cy}, respectively. Thus, the proposed HIE-FDTD formulas only contain graphene parameters in the graphene cells, and only contain BP parameters in the BP cells.

Optics EXPRESS

2.4. Conformal HIE-FDTD for curved boundaries

The staircasing approach to simulate curved objects with the conventional FDTD method not only introduces errors but also generate spurious solutions. In the past few decades, numerous methods have been proposed to analyze curved objects in order to overcome these difficulties, notably the conformal FDTD method by [47]. In spite of this, the conformal FDTD technique [31] is hybridized with the proposed HIE-FDTD method to accurately model the graphene and BP sheet with cured boundaries. For two-dimension materials located in the x-y plane, the conformal HIE-FDTD technique is only need to implement in the x-y plane. Thus, we only need to calculate the effective conductivity in cells filled with different materials. In this way, the updated effective conductivity for conformal HIE-FDTD method can be directly implemented by modifying coefficients S_2, S_3, C_2 and C_3 as follows

$$S_2 = \frac{l_x\sigma_0\Delta t}{\Delta x(2\tau+\Delta t)d}, \quad S_3 = \frac{l_y\sigma_0\Delta t}{\Delta y(2\tau+\Delta t)d}$$
$$C_2 = -\frac{l_x\Delta t\sigma_{cx}}{\Delta x(2\hbar-\Delta t\eta)h}, \quad C_3 = -\frac{l_y\Delta t\sigma_{cy}}{\Delta y(2\hbar-\Delta t\eta)h}$$

where l_x and l_y are the grid lengths outside the graphene/BP in the partially-filled cell, along the x- and y-directions, respectively. Δx and Δy are the step sizes along the x- and y-directions, respectively. In this way, this new approach improves the accuracy of the dispersive and anisotropic HIE-FDTD method while with the same costs in terms of central processing unit (CPU) time and memory.

3. Numerical analysis

The infinite graphene-BP layer is simulated in this section to verify the capability of the anisotropic HIE-FDTD method in simulating the graphene-BP based structure. In the following numerical experiments, the uniform plane wave is introduced to the HIE-FDTD method. The transmission coefficient of the structure is calculated, and compared with the conventional FDTD method. Based on this method, we propose a novel multi-layer GBP-DATAS and analyze its optical characteristics in different physical and geometrical parameters.

3.1. Numerical validation of the anisotropic HIE-FDTD scheme

In order to verify the accuracy of the anisotropic HIE-FDTD method in simulating graphene and BP structure, infinite monolayer graphene and BP sheets: in free space are simulated here. As shown in Fig. 1, infinite graphene and BP sheets are located in the x-y plane from top to bottom, with a distance setting to 180 nm. The thickness of the graphene and BP sheet are both 5 nm. For graphene layer, μ_c is taken as 0.5 eV, τ is taken as 0.3 ps, and the temperature T is assumed to be 300 K [48]. For BP layer, η is taken as 10 emV, n_s is taken as 2×10^{13} cm^{-2}, and the scale length of the BP a is taken as 0.2 nm [49]. The polarized electric field in the x-direction is normally incident on these two sheets. The uniform plane wave is introduced through the total-field/scattered-field (TF/SF) boundary condition. The perfectly matched layer (PML) is added on the top and bottom surface of the model to simulate open space in the z-direction, and the periodic boundary conditions are added in the x- and y-directions. In the anisotropic HIE-FDTD method, the spatial cell size Δz =1 nm is selected to discretize the graphene and BP sheets in the z-direction, and the 0.2 um uniform cells are used to discretize the rest of the space. In order to achieve the same accuracy, the spatial cell sizes of conventional FDTD method shall be taken as Δx =Δy =Δz=1 nm. According to the CFL condition, the maximum time step shall be $\Delta t \le 1/\left(c\sqrt{1/\Delta x^2+1/\Delta y^2+1/\Delta z^2}\right) = 3.33\times10^{-6}ps$. However, for the HIE-FDTD method, the maximum time step shall be $\Delta t \le 1/\left(c\sqrt{1/\Delta x^2+1/\Delta y^2}\right) = 2.35\times10^{-4}ps$, which is 70 times

Optics EXPRESS

as that of the conventional FDTD method. The transmission coefficient of the graphene-BP sheets calculated by the HIE-FDTD is in good agreement with the simulation result calculated by the conventional FDTD method, as shown in Fig. 2. It verifies that the HIE-FDTD method has high computational accuracy. The computational time for the FDTD method and the HIE-FDTD method are 8912 and 216 seconds, respectively. The computational time of the HIE-FDTD scheme is only 1/41 times as that of the conventional FDTD method. Therefore, the proposed HIE-FDTD method for graphene and BP simulation has obvious advantages and high efficiency.

3.2. Simulation of the terahertz absorption structure

In this section, a novel sub-wavelength plasmonic graphene-BP-based dual-band anisotropic terahertz absorption structure (GBP-DATAS) is proposed, which consists of two groups of nanodisk absorbers with different radius. The distance between these two groups and the thickness of top dielectric layer are both t = 3.78 μm, as shown in Fig. 3.

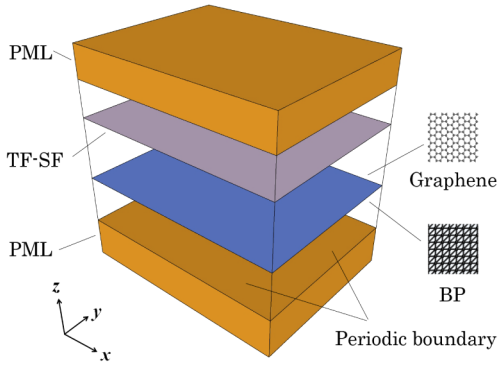

Fig. 1. Geometry of the computation domain including infinite monolayer graphene and BP sheets

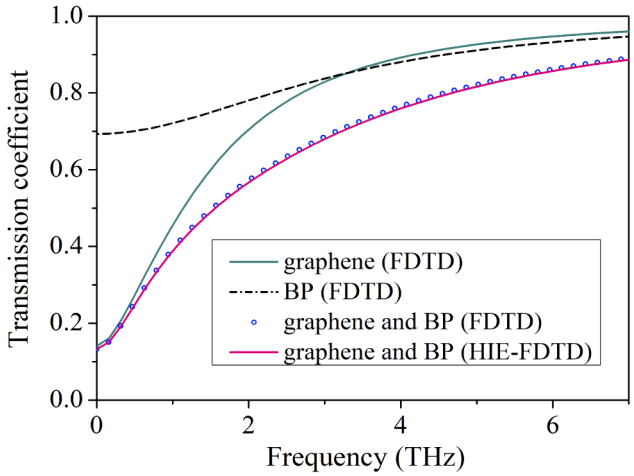

Fig. 2. Transmission coefficients of the graphene and BP sheets calculated by the FDTD and HIE-FDTD methods.

Each group of nanodisks consist of stacked graphene-BP bilayer supported by Al_2O_3 layers with a relative permittivity of 3.2. A layer of hexagonal boron nitride (*h*BN) is placed between the graphene and BP sheets as isolation spacers to maintain high carrier mobility and prevent carrier

Optics EXPRESS

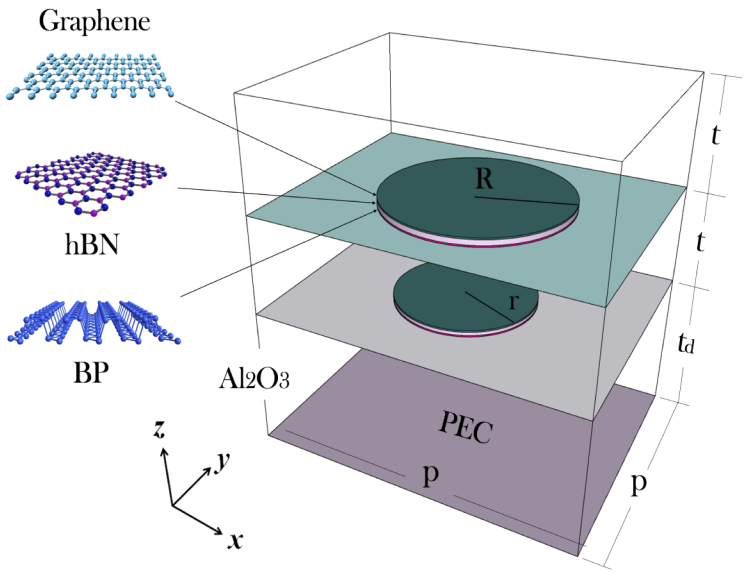

Fig. 3. Geometry of the proposed graphene-BP-based dual-band anisotropic terahertz absorption structure (GBP-DATAS).

transport between the graphene and BP [50]. The impact of top dielectric layer on absorption spectrum can be neglected because its thickness t is far smaller than the incident wavelength.

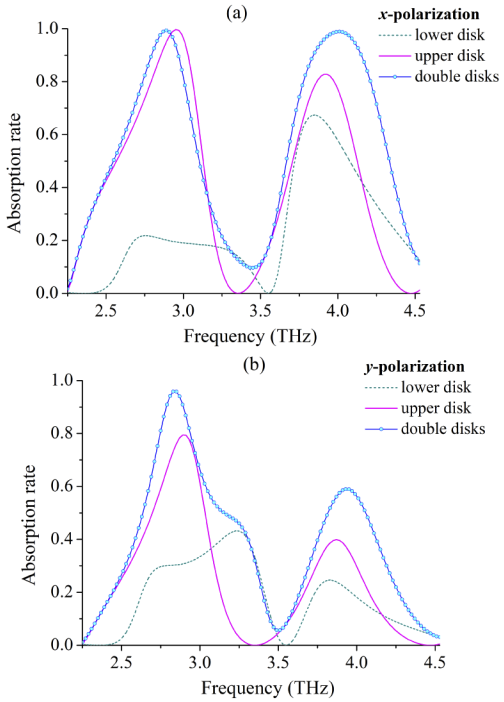

Fig. 4. Absorption rate of two-layer graphene/BP nanodisk and the GBP-DATAS under (a) *x*-polarization and (b) *y*-polarization.

Optics EXPRESS

However, the dielectric layer can protect top bimolecular graphene-BP layer against damage from environment to ensure highly stable operation of the GBP-DATAS in different environment within a long period. In order to study the absorption features of the GBP-DATAS, we simulate and analyze the proposed model with conformal technology applicable to curved structure and with in-plane anisotropic HIE-FDTD algorithm based on the Drude model and the ADE technique. In the computational domain of anisotropic HIE-FDTD method, the periodic boundary conditions are used in the x- and y-directions, while PML and PEC boundary conditions are used at the top and the bottom, respectively. This periodic structure is set with the length and the width p=9 μm, and the thickness of bottom dielectric layer is t_d=60 μm. The top and bottom nanodisks are set with radius R=4.32 μm and r=2.16 μm, respectively. The thickness of the hBN layers between graphene and BP are both 180 nm, and the thickness of graphene and BP layers are both 5 nm. The uniform plane waves in the terahertz band are introduced via TF/SF boundary condition and normally incident to the GBP-DATAS. In order to effectively simulate photoelectric properties of the model, in-plane anisotropic HIE-FDTD method is used to simulate the structure involving both graphene and BP. Moreover, conformal technology applicable to anisotropic HIE-FDTD method is used to accurately simulate 2DMs with curved structure. Generally, absorption rate can be expressed as A=1-T-R, transmission coefficient is $T = |S_{21}|^2$ and reflection coefficient is $R = |S_{11}|^2$, where S is the scattering parameter. Since the PEC is applied in the bottom surface, the transmission is equal to 0, thus the expression of absorption rate can be simplified to A=1-R. In order to analyze the absorption features of the GBP-DATAS,we first investigate the absorption rates of a single nanodisk and dual nanodisks with incident lights in different polarizations. as shown in Fig. 4. It can be seen from Fig. 4(a) that when polarized plane waves in the x-direction are normally incident, the absorption peaks of the top nanodisk and dual nanodisk structure appear around 3 THz and 4 THz respectively, but the absorption rate of the bottom nanodisk

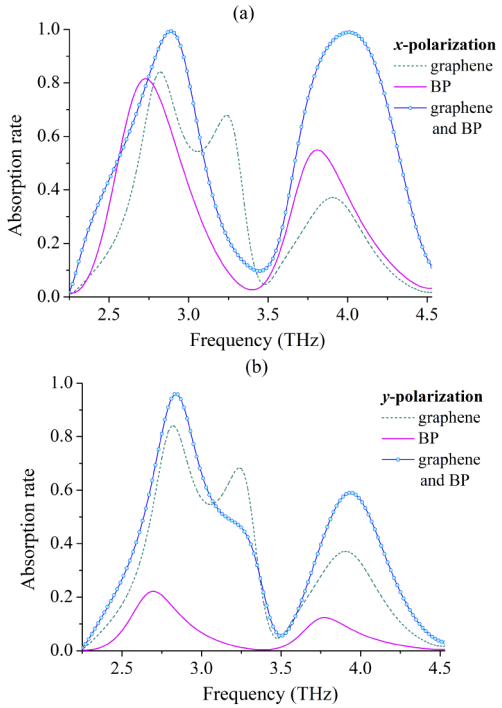

Fig. 5. Absorption rate of two-layer graphene/BP nanodisk and the GBP-DATAS under (a) x-polarization and (b) y-polarization.

Optics EXPRESS

structure is relatively weak. Note that the absorption rate of the dual nanodisk exceeds 99%, forming a perfect absorber with dual resonance. On the other hand, when polarized plane waves in the *y*-direction are normally incident, as shown in Fig. 4(b), the absorption peaks of the top nanodisk and dual nanodisk structure also appear around 3 THz and 4 THz respectively, but the absorption rate of the bottom nanodisk structure is still weak. Relatively, the absorption rate of the dual nanodisk structure is the strongest. It exceeds 95% at 3 THz and reaches over 60% at 4 THz. Different absorption effects can be obtained under the excitation of different polarized plane waves due to the addition of the BP. The excitation source will generate local surface plasmonic in the graphene-BP nanoparticles with finite length. However, there is a significant difference in the absorption effect of light when different effective masses in BP are excited under different polarized waves, finally forming anisotropic feature of the GBP-DATAS. When the free space and GBP-DATAS accommodate impedance matching conditions, the absorption rate will tend to 100%. Therefore, it is possible to design reflective polarizers or polarized optical filters working in different frequency regions based on the absorption capacity of the proposed GBP-DATAS. To further analyze the absorption characteristics of the GBP-DATAS, we compare two-layer graphene nanodisk and two-layer BP nanodisk structure with the GBP-DATAS, and show significant difference in the absorption rate and slightly shift of the absorption peak, as shown in Fig. 5. If there are only two layers of graphene nanodisks, optical response is not sensitive to the incident polarization due to the isotropic surface conductivity of the graphene. If there are only two layers of BP nanodisks, weak optical resonance may occur under the excitation of different incident polarization. This polarized dependence is determined by anisotropic plasmonic dispersion of the BP. However, combined with the advantages of graphene and BP, the GBP-DATAS has strong anisotropic plasmonic resonance. Specifically, for polarized incident wave in *x*-direction, as shown in Fig. 5(a), the absorption rate of the two-layer graphene nanodisk structure reaches up to 80% around 2.8 THz and is lower than 40% around 3.9 THz. When BP sheet is added, the shift of the absorption peaks occurs in the GBP-DATAS. The first peak is blue-shifted from 2.7 THz to 2.9 THz and the absorption rate increases to 99%. The second peak is also blue-shifted from 3.8 THz to 4.0 THz and the absorption rate increases to 98%. For polarized incident wave in *y*-direction, the absorption rates of GBP-DATAS under dual resonance increase 11% and 21% respectively compared to the two-layer graphene nanodisks, and increase 72% and 47% respectively compared to the two-layer BP nanodisks. It is noted that the absorption of graphene nanodisks with incident lights in different polarizations is unchanged because of the isotropic of graphene. However, due to the existence of BP layer, GBP-DATAS has a significant anisotropic feature and higher absorption rate compared to pure graphene nanodisks. Finally, to further study the influence of structural size on absorption feature, we investigate the changes of radius R of top-layer nanodisk on GBP-DATAS (R1=1.8 μm, R2=2.16 μm, R3=2.52 μm, R4=2.88 μm, R5=3.24 μm, R6=3.6 μm, R7=3.96 μm, and R8=4.32 μm), and thickness t between two nanodisks (t1=2.88 μm, t2=3.24 μm, t3=3.6 μm, t4=3.96 μm, and t5=4.32 μm) to study absorption characteristics of GBP-DATAS under polarized incident lights in *x*-direction, as shown in Fig. 6. It can be seen from Fig. 6(a) that radius R of top-layer nanodisk will influence left absorption peak. As radius increases from R1 to R8, the left absorption peak is first red-shifted and then blue-shifted, and the absorption rate finally increases to 99%. This phenomenon can be attributed to the fact that, normally, the resonant wavelength of the electric dipole resonance induced in the top-layer nanodisk is proportional to its radius, thus the redshift happens as the radius increases. However, when the radius increases to a certain value, the periodic spacing between adjacent nanodisks will be less than the critical coupling distance, then the coupling between adjacent graphene-BP nanodisks will be relatively strong. Therefore, the coupling effect between adjacent dipoles leads to the broader bandwidth and then the blueshift [51], as shown in Fig. 6(a). The changes of radius r of bottom-layer nanodisk will affect the right absorption peak, which is not discussed any more here. In addition, changing the distance t between two

Optics EXPRESS

nanodisks will influence the shifting of the dual-resonance peaks, as shown in Fig. 6(b). As distance increases from t1 to t5, dual-resonance peaks are blue-shifted, but the absorption rate is almost unchanged. Because strong plasmonic resonance occurs in graphene-BP layer, incident light will be highly concentrated around the graphene-BP layer and optical loss is mainly gathered here. Therefore, the thickness t of the dielectric layer has few influence on the absorption rate.

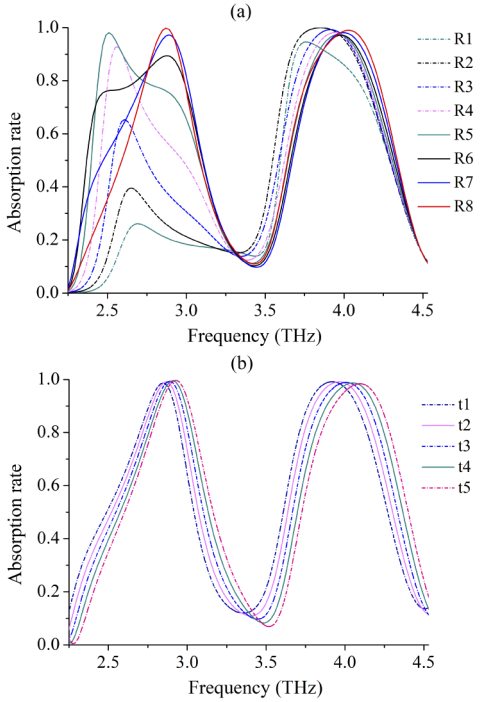

Fig. 6. Absorption rate of the GBP-DATAS under normal incident light with structural parameters (a) changing radius R of top-layer nanodisk (b) changing thickness t between two nanodisks.

4. Conclusion

Through combining ADE technique with surface conductivity of graphene and black phosphorus (BP), this paper proposes a novel anisotropic HIE-FDTD method which makes possible for simulation of optical devices containing graphene and BP in the terahertz band. Compared to the conventional FDTD method, the proposed method can greatly reduce calculation time and memory consumption, indicating higher computational efficiency. With this method, we present a multi-layer GBP-DATAS and successfully analyze its optical features. Combining the advantages of graphene and BP localized surface plasmons, the GBP-DATAS demonstrates strong anisotropic plasmonic resonance, which are available in neither individual graphene nor BP sheets. In addition, the proposed GBP-DATAS has an extremely high anisotropic absorption rate and therefore can be used to design novel terahertz sensors and tunable reflective polarizer in symmetrical structure.

Funding. Natural Science Basic Research Program of Shaanxi Province (2020JM-515); Key Research and Development Projects of Shaanxi Province (2018GY-151); Natural Science Foundation of Fujian Province (2020J01294).

Acknowledgment. We gratefully acknowledge the help of Dr. Y. Guo and H. Zhang for their valuable discussions and suggestions. We also thank Ms. Y. Chen for the language check, and anonymous referees for their comments that greatly improved the paper.

Optics EXPRESS

Disclosures. The authors declare that there are no conflicts of interest related to this article.

Data availability. The data that support the findings of this study are available from the corresponding author upon reasonable request.

References

1. K. S. Novoselov, D. Jiang, F. Schedin, T. J. Booth, V. V. Khotkevich, S. V. Morozov, and A. K. Geim, "Two-dimensional atomic crystals," Proc. Natl. Acad. Sci. U. S. A. **102**(30), 10451–10453 (2005).
2. F. Xia, W. Han, X. Di, M. Dubey, and A. Ramasubramaniam, "Two-dimensional material nanophotonics," Nat. Photonics **8**, 899–907 (2014).
3. T. Low and P. Avouris, "Graphene plasmonics for terahertz to mid-infrared applications," ACS Nano **8**(2), 1086–1101 (2014).
4. P. Y. Chen and A. Alu, "Terahertz metamaterial devices based on graphene nanostructures," IEEE Trans. Terahertz Sci. Technol. **3**(6), 748–756 (2013).
5. H. J. Li, L. L. Wang, J. Q. Liu, Z. R. Huang, B. Sun, and Z. Xiang, "Investigation of the graphene based planar plasmonic filters," Appl. Phys. Lett. **103**(21), 211104 (2013).
6. S. He and T. Chen, "Broadband thz absorbers with graphene-based anisotropic metamaterial films," IEEE Trans. Terahertz Sci. Technol. **3**(6), 757–763 (2013).
7. L. Wang, X. Chen, A. Yu, Y. Zhang, J. Ding, and W. Lu, "Highly sensitive and wide-band tunable terahertz response of plasma waves based on graphene field effect transistors," Sci. Rep. **4**(1), 5470 (2015).
8. Z. H. Zhu, C. C. Guo, K. Liu, J. F. Zhang, and S. Q. Qin, "Electrically controlling the polarizing direction of a graphene polarizer," J. Appl. Phys. **116**(10), 104304 (2014).
9. Y. Cai, K. D. Xu, N. Feng, R. Guo, and J. Zhu, "Anisotropic infrared plasmonic broadband absorber based on graphene-black phosphorus multilayers," Opt. Express **27**(3), 3101–3112 (2019).
10. J. Zhang, Z. H. Zhu, W. Liu, X. Yuan, and S. Q. Qin, "Towards photodetection with high efficiency and tunable spectral selectivity: graphene plasmonics for light trapping and absorption engineering," Nanoscale **7**(32), 13530–13536 (2015).
11. Y. Chen, G. Jiang, S. Chen, Z. Guo, X. Yu, C. Zhao, H. Zhang, Q. Bao, S. Wen, and D. Tang, "Mechanically exfoliated black phosphorus as a new saturable absorber for both q-switching and mode-locking laser operation," Opt. Express **23**(10), 12823–12833 (2015).
12. L. Li, Y. Yu, G. J. Ye, Q. Ge, X. Ou, H. Wu, D. Feng, X. H. Chen, and Y. Zhang, "Black phosphorus field-effect transistors," Nat. Nanotech. **9**, 372–377 (2014).
13. Low Tony, Roldan Rafael, Wang Han, Xia Fengnian, and Avouris Phaedon, "Plasmons and screening in monolayer and multilayer black phosphorus," Phys. Rev. Lett. (2014).
14. H. F. M. Y. M. Qing and T. J. Cui, "Tailoring anisotropic perfect absorption in monolayer black phosphorus by critical coupling at terahertz frequencies," Opt. Express **26**(25), 32442–32450 (2018).
15. Wang Jiao, Jiang Yannan, and Hu Zhirun, "Dual-band and polarization-independent infrared absorber based on two-dimensional black phosphorus metamaterials," Opt. Express **25**(18), 22149–22157 (2017).
16. W. Xi, M. Qian, L. Wu, J. Guo, S. Lu, X. Dai, and Y. Xiang, "Tunable terahertz/infrared coherent perfect absorption in a monolayer black phosphorus," Opt. Express **26**(5), 5488 (2018).
17. D. T. Debu, D. F. S. J. Bauman, H. O. H. Churchill, and J. B. Herzog, "Tuning infrared plasmon resonance of black phosphorene nanoribbon with a dielectric interface," Sci. Rep. **8**(1), 3224 (2018).
18. J. Nong, W. Wei, W. Wei, G. Lan, and L. Tang, "Strong coherent coupling between graphene surface plasmons and anisotropic black phosphorus localized surface plasmons," Opt. Express **26**(2), 1633 (2018).
19. H. F. M. Y. M. Qing and T. J. Cui, "Strong coupling between magnetic plasmons and surface plasmons in a black phosphorus-spacer-metallic grating hybrid system," Opt. Lett. (2018).
20. C. Fang, Y. Liu, G. Han, Y. Shao, J. Zhang, and Y. Hao, "Localized plasmon resonances for black phosphorus bowtie nanoantennas at terahertz frequencies," Opt. Express **26**(21), 27683–27693 (2018).
21. Q. Hong, X. Feng, X. Wei, Z. Zhu, K. Liu, X. Yuan, J. Zhang, and S. Qin, "Towards high performance hybrid two-dimensional material plasmonic devices: strong and highly anisotropic plasmonic resonances in nanostructured graphene-black phosphorus bilayer," Opt. Express **26**(17), 22528 (2018).
22. G. D. Bouzianas, N. V. Kantartzis, C. S. Antonopoulos, and T. D. Tsiboukis, "Optimal modeling of infinite graphene sheets via a class of generalized fdtd schemes," IEEE Trans. Magn. **48**(2), 379–382 (2012).
23. W. H. Weedon and C. M. Rappaport, "A general method for fdtd modeling of wave propagation," IEEE Trans. Antennas Propag. **45**(3), 401–410 (1997).
24. A. Mock, "Pade approximant spectral fit for fdtd simulation of graphene in the near infrared," Opt. Mater. Express **2**(6), 771–781 (2012).
25. H. Lin, M. F. Pantoja, L. D. Angulo, J. Alvarez, R. G. Martin, and S. G. Garcia, "Fdtd modeling of graphene devices using complex conjugate dispersion material model," IEEE Microw. Wirel. Components Lett. **22**(12), 612–614 (2012).
26. B. Salski, "An fdtd model of graphene intraband conductivity," IEEE Trans. Microwave Theory Tech. **62**, 1570–1578 (2014).
27. J. Chen, X. Ning, A. Zhang, and J. Guo, "Using dispersion hie-fdtd method to simulate the graphene-based polarizer," IEEE Trans. Antennas Propag. **64**(7), 3011–3017 (2016).

Optics EXPRESS

28. X. Ning, J. Chen, J. Wang, X. Qin, and J. Shi, "Dispersion hie-fdtd method for simulating graphene-based absorber," IET Microwaves, Antennas Propag. **11**(1), 92–97 (2017).
29. J. Chen and J. Wang, "Three-dimensional dispersive hybrid implicit"cexplicit finite-difference time-domain method for simulations of graphene," Comput. Phys. Commun. **207**, 211–216 (2016).
30. D. D. Z. A. V. Londersele and D. V. Ginste, "Full-wave analysis of the shielding effectiveness of thin graphene sheets with the 3d unidirectionally collocated hie-fdtd method," Int. J. Antennas Propagation **2017**, 1–8 (2017).
31. M. L. Zhai, H. L. Peng, X. H. Wang, X. Wang, Z. Chen, and W. Y. Yin, "The conformal hie-fdtd method for simulating tunable graphene-based couplers for thz applications," IEEE Trans. Terahertz Sci. Technol **5**(3), 368–376 (2015).
32. J. Chen, J. Li, and Q. H. Liu, "Designing graphene-based absorber by using hie-fdtd method," IEEE Trans. Antennas Propag. **65**(4), 1896–1902 (2017).
33. M. L. Zhai, H. L. Peng, J. F. Mao, and W. Y. Yin, Modeling tunable graphene-based filters using leapfrog adi-fdtd method, in *2015 IEEE MTT-S International Microwave Workshop Series on Advanced Materials and Processes for RF and THz Applications (IMWS-AMP)* (2015).
34. X. H. Wang, W. Y. Yin, and Z. Z. Chen, "One-step leapfrog adi-fdtd method for simulating electromagnetic wave propagation in general dispersive media," Opt. Express **21**(18), 20565–20576 (2013).
35. I. Ahmed, E. H. Khoo, and E. Li, "Efficient modeling and simulation of graphene devices with the lod-fdtd method," IEEE Microw. Wirel. Compon **23**(6), 306–308 (2013).
36. N. V. Kantartzis, T. Ohtani, and Y. Kanai, "Accuracy-adjustable nonstandard lod-fdtd schemes for the design of carbon nanotube interconnects and nanocomposite emc shields," IEEE Trans. Magn. **49**(5), 1821–1824 (2013).
37. R. Zhou, J. Peng, S. Yang, D. Liu, Y. Xiao, and G. Cao, "Lifetime and nonlinearity of modulated surface plasmon for black phosphorus sensing application," Nanoscale **10**(39), 18878–18891 (2018).
38. W. Lei, T. Zhang, P. Liu, J. A. Rodriguez, G. Liu, and M. Liu, "Bandgap- and local field-dependent photoactivity of ag/black phosphorus nanohybrids," ACS Catal. **6**(12), 8009–8020 (2016).
39. Mamiki and Takefumi, A new fdtd algorithm based on alternating-direction implicit method," IEEE Trans. Microwave Theory Tech (1999).
40. W. Zhu, C. Ji, and Y. Chen, "Development of a higher-order adi-fdtd method," Microw. Opt. Technol **37**(1), 8–12 (2003).
41. Y. Yang, R. S. Chen, and E. Yung, "The unconditionally stable crank nicolson fdtd method for three–dimensional maxwell's equations," Microw. Opt. Technol. Lett. **48**(8), 1619–1622 (2006).
42. M. Unno and H. Asai, "Hie-fdtd method for hybrid system with lumped elements and conductive media," Microw. Wirel. Components Lett. IEEE **21**(9), 453–455 (2011).
43. L. Li, H. Zhang, X. Han, N. H. Muhammad, and Y. Zhou, "A hybrid implicit-explicit fdtd method for simulation of ultra-wideband bandpass filter," in *2019 PhotonIcs and Electromagnetics Research Symposium - Spring (PIERS-Spring)* (2019).
44. M. L. Zhai, H. L. Peng, W. Y. Yin, and Z. Chen, "Hie-fdtd method for simulating tunable terahertz graphene absorber," in *2015 IEEE International Symposium on Antennas and Propagation and USNC/URSI National Radio Science Meeting* (2015).
45. J. Chen and J. Wang, "A three-dimensional semi-implicit fdtd scheme for calculation of shielding effectiveness of enclosure with thin slots," IEEE Trans. Electromagn. Compat. **49**(2), 354–360 (2007).
46. J. Chen and J. Wang, "Numerical simulation using hie-fdtd method to estimate various antennas with fine scale structures," IEEE Trans. Antennas Propag. **55**(12), 3603–3612 (2007).
47. W. Yu and R. Mittra, "A conformal finite difference time domain technique for modeling curved dielectric surfaces," IEEE Microw. Wirel. Components Lett. **11**, 25–27 (2001).
48. Y. Jiang, H. D. Zhang, J. Wang, C. N. Gao, J. Wang, and W. P. Cao, "Design and performance of a terahertz absorber based on patterned graphene," Opt. Lett. **43**(17), 4296–4299 (2018).
49. Z. C. Luo, M. Liu, Z. N. Guo, X. F. Jiang, A. P. Luo, C. J. Zhao, X. F. Yu, W. C. Xu, and H. Zhang, "Microfiber-based few-layer black phosphorus saturable absorber for ultra-fast fiber laser," Opt. Express **23**(15), 20030 (2015).
50. T. Ishii and T. Sato, "Growth of single crystals of hexagonal boron nitride-sciencedirect," J. Cryst. Growth **61**(3), 689–690 (1983).
51. Y. Cai and K. Xu, "Tunable broadband terahertz absorber based on multilayer graphene-sandwiched plasmonic structure," Opt. Express **26**(24), 31693–31705 (2018).